INTERNATIONAL JOURNAL OF AMBIENT ENERGY
2023, VOL. 44, NO. 1, 703–718
https://doi.org/10.1080/01430750.2022.2142285

Taylor & Francis
Taylor & Francis Group

Energy management of a DC microgrid with hybrid energy storage system using PI and ANN based hybrid controller

Amit Kumar Rajput and J. S. Lather

Department of Electrical Engineering, National Institute of Technology, Kurukshetra, India

ABSTRACT

An energy management system incorporating a hybrid control scheme based on artificial neural networks (ANN)-based controller and a classical proportional–integral (PI) controller is proposed for a DC microgrid (DCMG) consisting of a fuel cell (FC) and a hybrid energy storage system (HESS) under variable load demand. The HESS incorporates a battery energy storage system (BESS) and a supercapacitor (SC) to cater high energy and high-power demands, respectively. The HESS with the proposed controller and energy management strategy (EMS) admits improved time response for sudden and slowly varying load demands, resulting in reduced battery stress with an improved battery life span. The microgrid configuration with a proposed hybrid controller is simulated on the Simulink® platform to establish its efficacy over a conventional controller. The proposed controller effectively minimises peak overshoot, settling time and deviation in DC bus voltage (DBV) , in comparison to the conventional one. Furthermore, simulation results are validated using a real-time OPAL-RT platform to ascertain effectiveness of the proposed strategy.

ARTICLE HISTORY
Received 12 November 2021
Accepted 17 October 2022

KEYWORDS
Artificial neural network; DC microgrid; Fuel cell; Hybrid energy storage system; Supercapacitor

1. Introduction

Microgrids incorporating renewable energy sources (RESs) are ubiquitous nowadays for their inherent advantages over their conventional counterparts. They provide an economical alternative to establishing transmission corridors in remote areas by harnessing renewable energy. Microgrids have been an environment-friendly alternative to fast-depleting fossil fuels. Microgrids harness RESs in remote areas near to loads and admit negligible transmission losses resulting in increased efficiency (Sahu et al. 2020b). In general, microgrids are of three types: AC, DC, and hybrid AC–DC. Presently, DCMGs are gaining popularity due to their low power loss, increased efficiency, improved reliability, ease of control requiring no synchronisation, absence of reactive power and easy interconnections to the utility (Vu et al. 2017). However, DCMGs suffer from power quality challenges such as voltage fluctuations, flickers, unwanted harmonics and load imbalance (Sahoo, Sinha, and Kishore 2018). The common cause of voltage fluctuations or flickers in standalone DCMG systems remains the integration of RESs such as wind and photovoltaic cells, as energy produced by such RESs is subject to weather conditions (Kathiresan, Natarajan, and Jothimani 2020). To address these issues, energy storage devices (ESDs) are employed in standalone microgrids to maintain a balance in generation and load demand, thereby improving the power quality of the microgrid system (Sahu et al. 2020c). A standalone microgrid comprising PV with a battery as ESD was proposed to balance the demand-generation gap amid uncertainties (Boujoudar et al. 2020), and an ANN controller was used to control the bidirectional DC/DC converter interlinking battery and DC bus. Despite the use of a fast ANN-based controller, the battery was unable to handle fast fluctuations in PV generation and load demand for its low power density, which resulted in increased stress on the battery (Rahman et al. 2020). A combination of different kinds of ESDs with diverse characteristics has been successful in addressing the aforesaid issue under similar situations (Bahloul and Khadem 2019; Xu et al. 2019). A combination of battery and SC is prevalent nowadays and is used in microgrids, electric vehicles and uninterruptible power supplies (Cabrane et al. 2021). Batteries are low power devices, whereas SCs are high power devices as shown in the Ragone plot in Figure 1 (Christen and Carlen 2000). The performance parameters with a comparison of these ESDs are summarised in Table 1.

EMS along with suitable controllers is required to keep the DBV regulated with balance in power mismatch between generation and demand met through HESS. A sliding mode controller (SMC) based on PWM for the boost converter controlling the PV generation in a DCMG consisting of PV and battery was proposed in (Singh and Lather 2018). However, the proposed control approach is difficult to design and relies heavily on device parameters. In (Chettibi et al. 2018), an adaptive neural network-based controller was reported to control hybrid AC–DC microgrid. Their proposed ANN-based controller swiftly tracks optimum power from RESs; however, EMS based on fuzzy logic control (FLC) approach was difficult to design with accuracy depending on the expert's prior domain knowledge. EMS for power sharing in an electric vehicle (EV) and FC-based microgrid with HESS was discussed in (Marzougui et al. 2019). The proposed strategy used FLC, flatness control and a rule-based algorithm and was overall complex and difficult to design. In (Fu et al. 2019), an EMS was proposed using hierarchical control to improve the

CONTACT Amit Kumar Rajput amit_61900141@nitkkr.ac.in

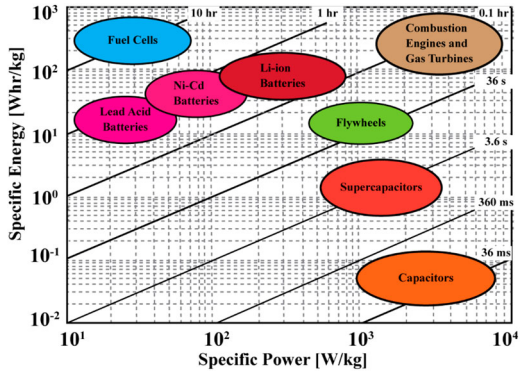

Figure 1. Ragone plot.

Table 1. Performance metric comparison of battery and SC (Glavin et al. 2008).

	SC	Battery
Charge/discharge efficiency	85–98%	70–85%
Cycle life	> 500,000	1,000
Discharge time	0.3–30 s	0.3–3 hr
Fast charge time	0.3–30 s	1–5 hr
Specific energy density	1–10 Wh/Kg	10–100 Wh/Kg
Specific power density	< 10000 W/Kg	< 1000 W/Kg

performance and fuel economy of hybrid EV. However, DBV regulation is not considered. The optimised operation and power management of a hybrid microgrid using a stochastic framework have been recently studied (Papari et al. 2019). However, control of power-sharing among various ESDs is not discussed. In (Sinha and Bajpai 2020), an adaptive FLC-based EMS for a standalone DCMG utilising RESs and HESS comprising battery and SC was proposed. The proposed strategy focuses on the over- and under-utilisation of ESD in a scenario with multiple ESDs. However, power-sharing among the various units of the microgrid is not discussed and FLC implementation depends on IF–THEN rules requiring a-prior information of the system. In (Sankar and Sekhar 2021), authors have compared three different configurations of microgrid i.e. with PV-battery /PV-FC and PV-FC-battery for performance testing, in terms of observed output power under uncertainty in PV power generation. However, DBV regulation is not highlighted and the battery is unable to cope with dynamic changes in demand or generated power. Power management for a low voltage DCMG using an ANN-based controller was reported in (Singh and Lather 2019) to control DC/DC converter interlinking battery and DC bus. For a DCMG consisting of a FC, PV and a battery, an ANN-based MPPT controller design and its performance were compared with regular perturb and observation methods (Pradhan et al. 2021). In literature, ANN controllers have been reported to be fast, stable, robust and resilient due to their parallel and distributed nature. In contrast, classical controllers like P, PI and PID are still the most extensively used in the industry due to their simple representation, ease of implementation, robustness due to model free nature, simple and frequent online retuning capabilities etc. In addition, the three parameters in PID can be independently adjusted to control the rise time, overshoot, steady-state error and settling time of the system (Mishra et al. 2021b; Nouman, Asim, and Qasim 2018). However, PID controllers may not achieve satisfactory performance in case of non-linearity or complex system structure. To address this issue, several researchers have supplemented conventional PID controllers with computational intelligence-based controllers resulting in hybrid controllers e.g. swarm and WOA optimisation based fuzzy, fuzzy-PID, combined PI-Sliding mode controller and ANFIS-PID controllers (Sahu et al. 2018; Sahu et al. 2020a; Mishra et al. 2021a; Singh and Lather 2020; Shaikh, AlGhamdi, and AlZaher 2018). The effectiveness of these hybrid controllers has motivated the present study of investigating a hybrid combination of an ANN controller with a PI controller to achieve improved results in terms of time response characteristics.

The proposed standalone DCMG configuration consists of a FC and HESS consisting of a battery and SC, where the surplus power of the FC is recycled using a battery as in (Xu et al. 2019). The objective of the present work remains to explore the use of hybrid control techniques to improve DC bus regulation with effective power sharing in DCMGs. To our best, hybrid PI and ANN-based control techniques for DCMG consisting FC, BESS and SC are not addressed in the literature yet. Here, the ANN-based hybrid controller along with EMS strategy is proposed for a grid-independent DCMG consisting of FC and HESS incorporating BESS and SC with the following objectives:

1. Effective power-sharing among various energy sources and HESS of the DCMG.
2. DBV (V_{DC}) regulation in the face of sudden changes in power generation/demand.
3. Regulation of the battery SOC to safeguard it from overcharging and deep-discharging.

The rest of the paper is structured as follows. The system configuration with modelling of the DCMG is described in Section 2. The proposed control strategy using hybrid control incorporating ANN-based and PI-based control loops is discussed in Section 3. The simulation results, experimental results and performance comparisons between the conventional and proposed controllers are presented in Section 4. The conclusion based on the study with future directions is discussed in Section 5.

2. System configuration and modelling

Figure 2(a,b) shows the considered configuration of standalone DCMG with load profile, HESS utilising battery and SC. The boost converter links FC to the DC bus, while SCs are linked to battery modules through a DC/DC buck–boost converter pair. The AC load is connected to the AC bus and is interlinked to the DC bus via a three-phase inverter. The controller pulls additional currents from HESS to maintain the V_{DC} and match the power requirements of the load, in case, generation falls short of those needs. The controller charges the HESS through surplus generation if generation exceeds load demand.

2.1. FC modelling

FCs are silent, portable and have efficiency up to 45%. Their versatility makes them ideal for small/micropower, transportation, large-scale fixed power systems and distributed power production (Dicks and Rand 2018).

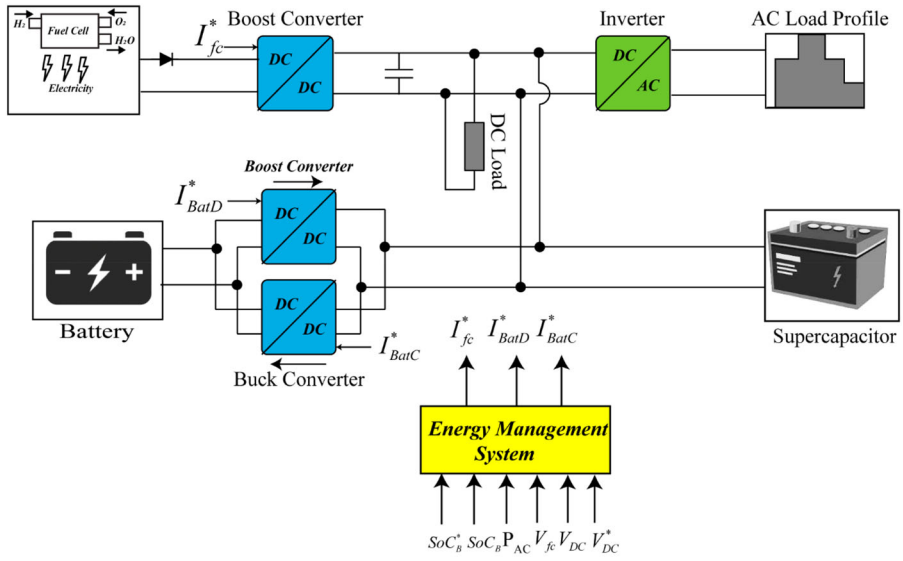

(a)

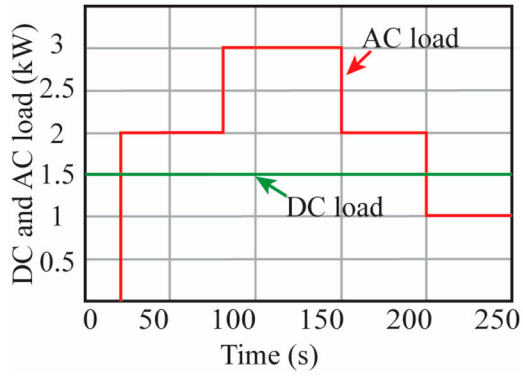

(b)

Figure 2. (a) Overall schematic of standalone DCMG (b) AC and DC load profile.

The cell output voltage relation is given by (Bracco et al. 2018)

$$E = E_{oc} - NA\ln\left(\frac{i_{fc}}{i_0}\right).\frac{1}{\frac{sT_d}{3}+1} \quad (1)$$

$$V_{fc} = E - R_{ohm}.i_{fc} \quad (2)$$

where, E_{oc} is open-circuit voltage, i_0 denotes exchange current (A), R_{ohm} is internal resistance (Ω), A denotes Tafel slope (in V), V_{fc} is FC voltage (in V), T_d denotes cell settling time (secs) and N denotes numbers of cells in series. Specifications of the FC model are listed in Table 2.

Table 2. Parameters of FC model.

Parameters	Specifications
Stack power	10.28 kW
Number of cells	65
Stack efficiency	50%
Resistance of FC	0.024535 Ω
System temperature	318 kelvins
Nominal air flow rate	732 lpm
Nominal fuel flow rate	114.9 lpm
NOMINAL CONSUMPTION	
Hydrogen (H_2)	98.98%
Oxidant (O_2)	42.88%
NOMINAL UTILISATION	
Air	269.5 slpm
Fuel	113.2 slpm

2.2. SC modelling

The operation of an SC is identical to a typical capacitor, but with a larger capacity and more energy storage. The SC model is based on the stern model, which is a hybrid of Helmholtz and Guoy–Chapman models. The capacitance relations of the SC are as follows:

$$C = \left[\frac{1}{C_H} + \frac{1}{C_{GC}}\right]^{-1} \quad (3)$$

$$C_H = \frac{N_e \in \in_0 A_i}{d} \quad (4)$$

$$C_{GC} = \frac{FQ_c}{2N_eRT}\sinh\left(\frac{Q_c}{N_e{}^2A_i\sqrt{8RT \in \in_0 C}}\right) \quad (5)$$

where C_H is Helmholtz capacitance; C_{GC} is Gouy-Chapman capacitance; $\in_0$ denotes permittivity of free space, $\in$ denotes permittivity of electrolyte material; A_i denotes inferential area between electrode and electrolyte; N_e denotes the number of

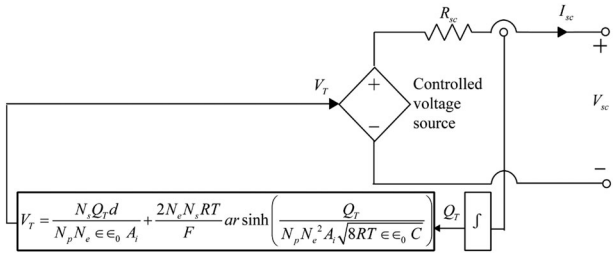

Figure 3. Equivalent circuit of SC.

Table 3. Parameters of SC model.

Parameters	Specifications
Rated capacitance	15.6 F
Number of capacitors in series	108
Number of capacitors in parallel	1
Equivalent DC series resistance	0.150 Ω

electrode layers; c is molar concentration and Q_c denotes electric charge of cell; The total capacitance of an SC module is given by

$$C_T = \frac{N_p}{N_s}.C \tag{6}$$

with losses in the resistance. SC Voltage is given as

$$V_{sc} = \frac{N_s Q_T d}{N_p N_e \in \in_0 A_i} + \frac{2N_e N_s RT}{F} ar\sinh \left(\frac{Q_T}{N_p N_e^2 \in \in_0 A_i \sqrt{8RT \in \in_0 C}} - i_{sc}.R_{sc} \right) \tag{7}$$

with

$$Q_T = \int i_{sc} dt \tag{8}$$

where N_s and N_p are the number of series and parallel cells, respectively; Q_T is electric charge; R_{sc} is total resistance of the SC module and i_{sc} is the current of the SC module. The model of SC is shown in Figure 3. Parameters of the utilised SC model have been enlisted in Table 3.

2.3. Battery modelling

The battery model based on the Shepherd curve fitting model is used in the proposed work. The voltage of battery can be written as

$$V_{\text{Bat}} = E_0 - K\left(\frac{Q}{Q-it}\right).it - iR_b - A_b e^{-B.it} - K\left(\frac{Q}{Q-it}\right).i^* \tag{9}$$

$$\text{SOC}_B = 100\left(1 - \frac{1}{Q}\int_0^t i(t)dt\right) \tag{10}$$

where E_0 is constant voltage of the battery (in V), K is polarisation constant (in Ah^{-1}), it denotes extracted capacity (in Ah), Q is the maximum capacity of the battery (in Ah), i^* is low-frequency current dynamics (in A), R_b is internal resistance of the battery, B is exponential capacity (in Ah^{-1}) and A_b is exponential voltage (in V). Parameters of the battery are tabulated in Table 4. Figure 4 shows the equivalent circuit of the battery.

Table 4. Parameters of battery.

Parameters	Specifications
Rated capacity	40 Ah
Nominal voltage	48 V
Internal resistance	0.012 Ω
Initial SOC	65%

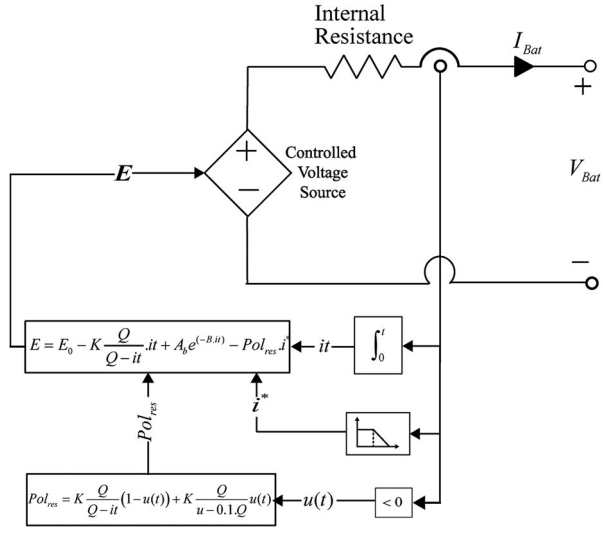

Figure 4. Equivalent circuit of battery.

2.4. DC/DC converter model

DC/DC converter connects FC and battery systems to DC bus, which allows and controls conversion of battery/ FC current and DBV (from low/high voltage to high/low voltage). DC/DC converters can be modelled as either a switching model or an average-value model. Such models are widely used for the purpose of accurate design along with the investigation of PWM switching harmonics and losses. However, the simulation of switching model-based DC/DC converters takes a considerably large simulation time. Figure 5(a,b), shows DC/DC converters used to interlink the battery with the DC bus. This converter pair employs a parallel combination of DC/DC isolated buck and boost converter for charging and discharging the battery. Converter interlinking FC to DC bus has an efficiency of 89.25%, while boost and buck converter pair has an efficiency of 87% and 87.97%, respectively.

2.5. PI controller for battery

PI controller regulates DBV by charging/ discharging the battery. If V_{DC} exceeds its reference value (V^*_{DC}), the PI controller sends a filtered reference current (I^*_{BatC}) signal to an isolated DC/DC buck-converter to charge the battery. If V_{DC} falls below V^*_{DC}, the PI controller sends reference current (I^*_{BatD}) to an isolated DC/DC boost converter for discharging the battery. PI controller for battery charging/discharging is shown in Figure 6.

2.6. Inverter modelling

Figure 7 shows the model of the inverter used. A three-phase 200 V, 400 Hz voltage signal is used as a reference for voltage-controlled sources. Input current is generated using DBV and the output power.

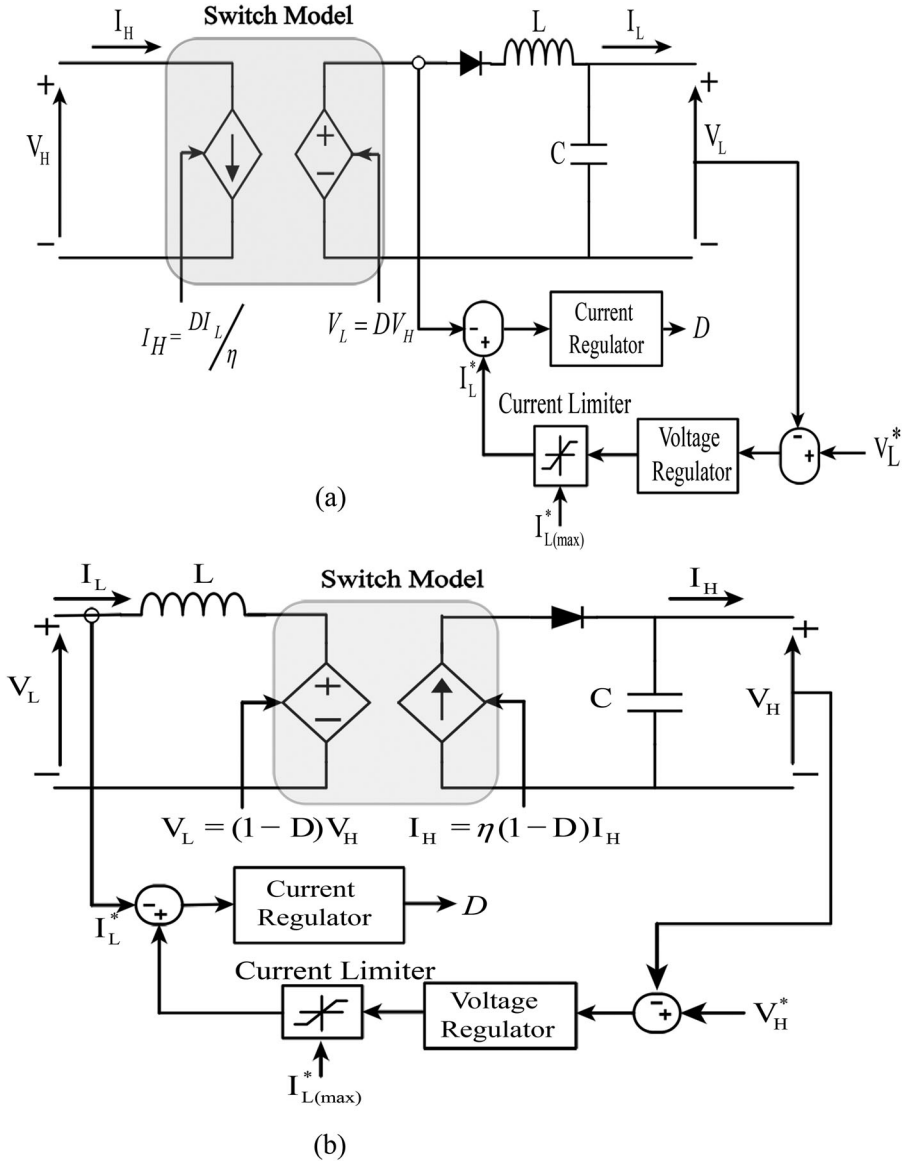

Figure 5. DC-DC converters (a) Buck (b) Boost.

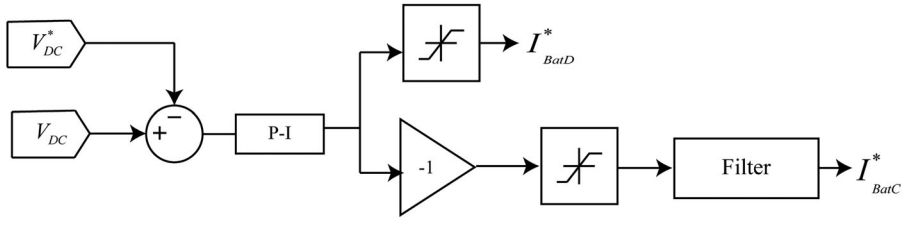

Figure 6. P-I controller for charging/discharging of battery.

3. Proposed control strategy

Figure 8(a), represents a block diagram of the conventional controller (Soumeur et al. 2020) while Figure 8(b) shows the schematics with the proposed controller. In a conventional control scheme, the PI controller is used for generating a current reference for FC. In contrast, the proposed control technique uses an ANN-based FC controller to control FC output for bridging the energy gap between load demand and ESDs.

3.1. Principle of ANN training

ANNs mimic biological neurons and provide a parallel and distributed computing architecture to model any general nonlinear (static as well as dynamic) relations between inputs and outputs. ANNs are able to learn these general relations in terms of weights and biases spread over multiple layers and nodes (artificial neurons). The input layer of ANN connects to system inputs and projects the weighted input signal to the next hidden

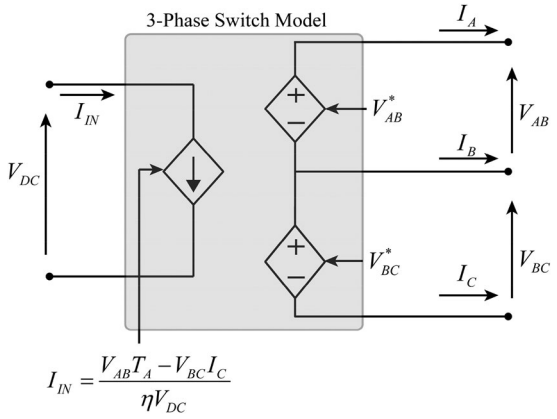

Figure 7. Inverter.

layer and so on. Finally, the output layer collects the weighted signals from the previous layer to produce ANN output. The ANN is trained using the Levenberg–Marquardt backpropagation learning technique, which effectively trains the model using a chain rule method. The output of n^{th} node in jth layer is calculated as (Brandt and Lin 1999)

$$x_n^{(j)} = f_n^{(j)}(net_n^{(j)}) = f_n^{(j)}\left(\sum_{i=1}^{N} w_i x_i^{(j-1)}\right) \tag{11}$$

where $f_n^{(j)}$ and $x_n^{(j)}$ represents the activation function and output of n^{th} node in j^{th} layer. w_i is connection weight from i^{th} input to n^{th} node, $x_i^{(j-1)}$ is i^{th} input of n^{th} node. N is the number of inputs to the j^{th} layer.

The objective of training is to minimise a quadratic cost function E, which is the sum of the square of errors in the output layer, as

$$E = \frac{1}{2}\left(\sum_{i=1}^{m} e_n^2\right) \tag{12}$$

where

$$e_n = x_n^{(j)} - d_n \tag{13}$$

Here, $x_n^{(j)}$ and d_n are the actual and desired outputs of n^{th} neuron, respectively. m represents the number of output neurons. Using the LM backpropagation learning technique, the weights are updated as

$$\begin{aligned}\Delta w_i &= f_n^{(j)'}(\text{net}_n^j)\frac{x_i^{(j-1)}}{x_n^j}\sum_{i=1}^{P} w_{ol}\Delta w_{ol} \\ &\quad - \gamma f_n^{(j)'}(\text{net}_n^{(j-1)})x_i^{(j-1)} e_n \Delta w_i \\ &= f_n^{(j)'}(\text{net}_n^j)\frac{x_i^{(j-1)}}{x_n^j}\end{aligned} \tag{14}$$

where $\gamma > 0$ is the coefficient of adaption and P denotes the number of neurons in the next layer. w_{ol} is the connection weight interlinking o^{th} neuron with I^{th} neuron.

Figure 9 shows schematics of the ANN-based controller. The hidden layer uses the following tan-sigmoidal function as activation:

$$x_i = f_n^{(j)}(\text{net}_n^{(j)}) = \frac{1 - e^{-\text{net}_n^{(j)}}}{1 + e^{-\text{net}_n^{(j)}}} \tag{15}$$

3.1.1. ANN-based FC controller

The proposed ANN controller configuration consists of three layers: an input layer, a hidden layer and an output layer. The input and output layers consist of one neuron each corresponding to single input and single output respectively, while the hidden layer consists of 10 neurons. In Figure 8(b), reference battery power is generated as the output of the ANN-based controller,

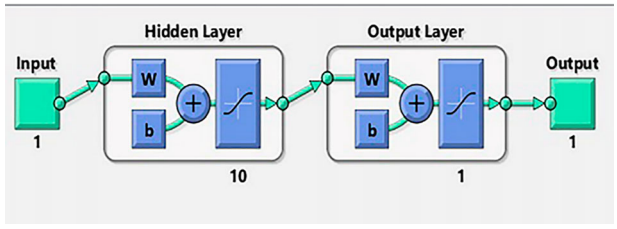

Figure 9. Network diagram of ANN controller.

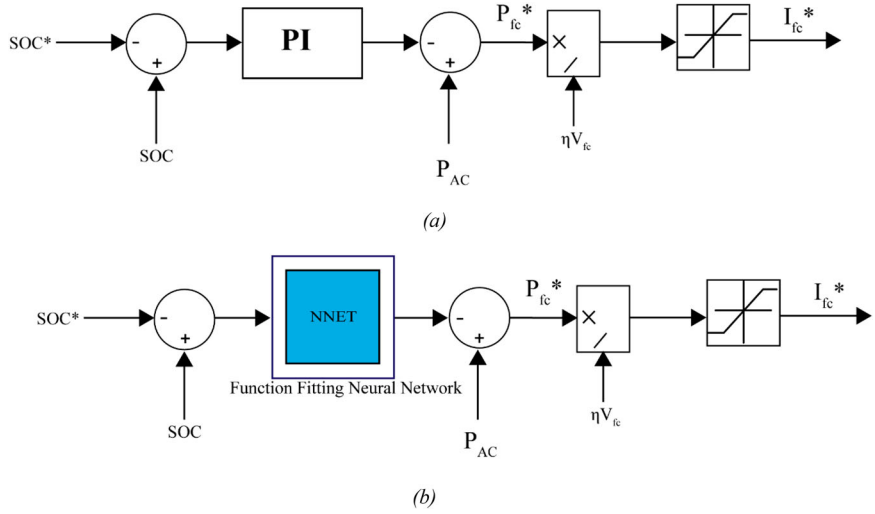

Figure 8. FC controller (a) Conventional controller (b) Proposed controller.

and is compared to AC load power to generate power reference for the FC. When SOC_B exceeds SOC_B^* the battery provides maximum power, and during this time, the FC power output is minimal. When SOC_B is less than SOC_B^*, FC provides major load power. The proposed ANN controller has been trained, tested and validated iteratively using 250000 data samples. The proposed controller is trained, tested and validated iteratively to optimise it using the deep learning toolbox of Matlab®. The training sample consists of 70% of available data, whereas the rest 30% of the available data is equally divided for testing and validation purpose samples, for which, the network diagram is shown in Figure 9. Regression R values measure how well outputs and goals match up. If the R value is 1, the relationship is close, and if it is 0, the relationship is random. The R value attained is 1 as shown in Figure 10, which validated that the data fits well and the controller is trained in the best possible manner. Figure 11 shows the overall training and testing accuracy of backpropagation classifier-trained neural network. The simulations were done using Matlab® on a desktop PC with Dell Optiplex 5050 with Intel 7th Generation i7-7700 CPU, 16 GB RAM with integrated Intel® HD 630 graphic processor. The HIL operations on OPAL-RT included Lenovo Laptop with 10th-generation Intel® i5 – 1035G1 CPU, 8GB RAM and integrated Intel® Iris® Xe graphics.

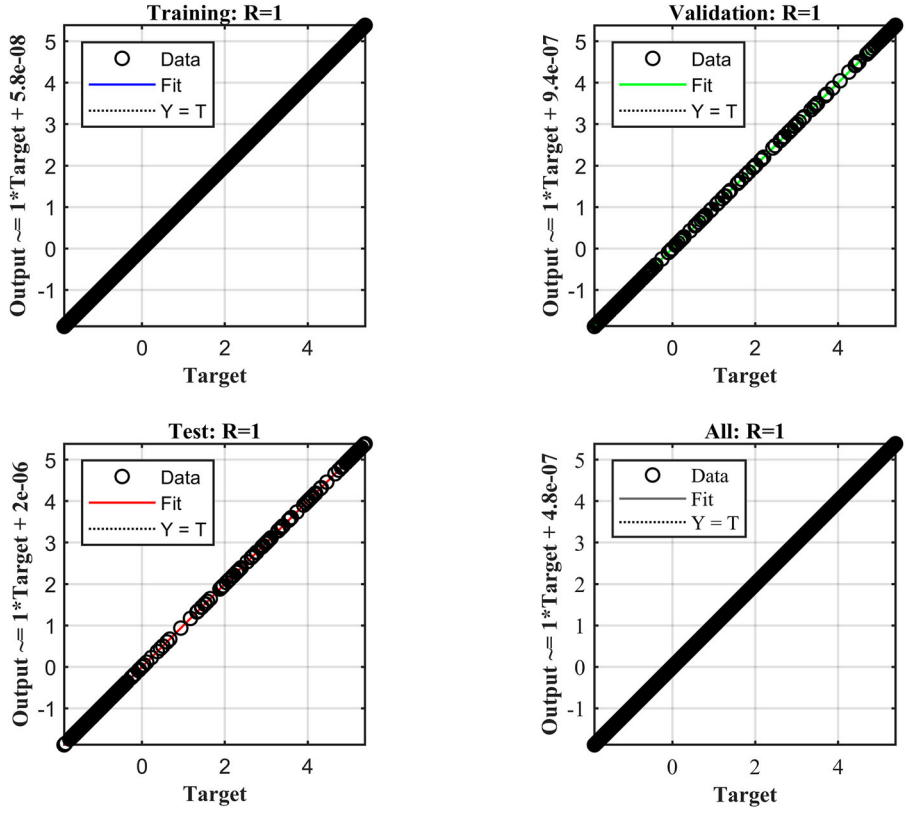

Figure 10. Training, validation, testing and set of all performance for ANN controller.

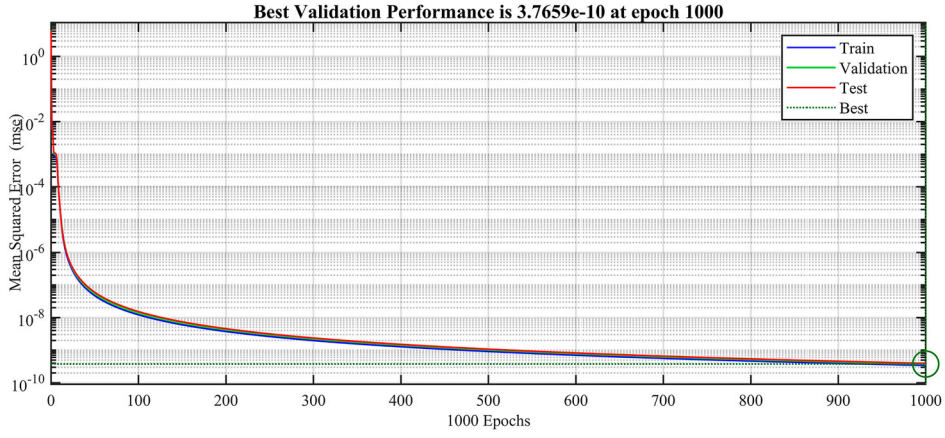

Figure 11. Best validation performance of ANN controller.

3.2. ANN-based energy management

The prime objective of an EMS is to maintain the power-balance between different DCMG units and load. Since the battery regulates DBV, SC power is not taken up in optimization problem formulation. As SC depletes, it is replenished from the battery and the AC load energy is solely shared between the battery and FC for any specific load cycle. The power balance considering losses can be given as

$$P_{FC} + P_{Bat} + P_{sc} - P_{Load} - P_{Loss} = 0 \tag{16}$$

Here,

$$P_{Load} = P_{AC} + P_{DC} \tag{17}$$

where P_{FC} is power generated by FC, P_{Bat} and P_{sc} are the power of battery and SC during charging/discharging. P_{Load}, P_{DC} and P_{AC} are total power and power consumed by DC and AC load. P_{Loss} represents the overall system losses.

The proposed EMS flowchart is shown in Figure 12. The EMS operating actions depend on the status of DBV and SOC_B. The EMS is designed in such a way that SOC_B remains inside boundaries, e.g. $20\% \leq SOC_B \leq 90\%$, respectively, and SC boundaries, e.g. $0\% \leq SOC_{sc} \leq 100\%$.

3.3. Real-time simulation of microgrid on RT-LAB

RT-LAB is a set of model-based test application platforms developed by Opal-RT. It divides the complex Simulink model into multiple subsystems that operate simultaneously. These subsystems can then be distributed across multiple CPU nodes to form a distributed and parallel real-time simulation system. The structure of the system is shown in Figure 13.

The proposed simulated model in Simulink environment is bifurcated into two subsystems named as *SM_subsystem* and *SC_subsystem*. The *SM_subsystem* is used for computations while the *SC_subsystem* is used as a graphical interface. The computation subsystems can further be divided into subsystems. Each computation subsystem is executed parallelly on a separate CPU core. Communication between computational subsystems is synchronous while that between computational subsystem and GUI subsystem is asynchronous. Figure 14 depicts the simulation flow of RT-Lab real-time simulation system. OpComm block is required to communicate between the computation and GUI subsystems. Fixed step solver is mandatory for real-time due to the lack of determinism in variable step solvers. Figure 15(a) shows the prepared model for RT-Lab in Matlab Simulink. Insight of the model under the *SM_subsystem* and the *SC_subsystem* is shown in Figure 15(b,c).

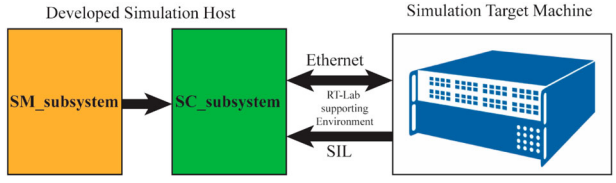

Figure 13. RT-Lab structure diagram.

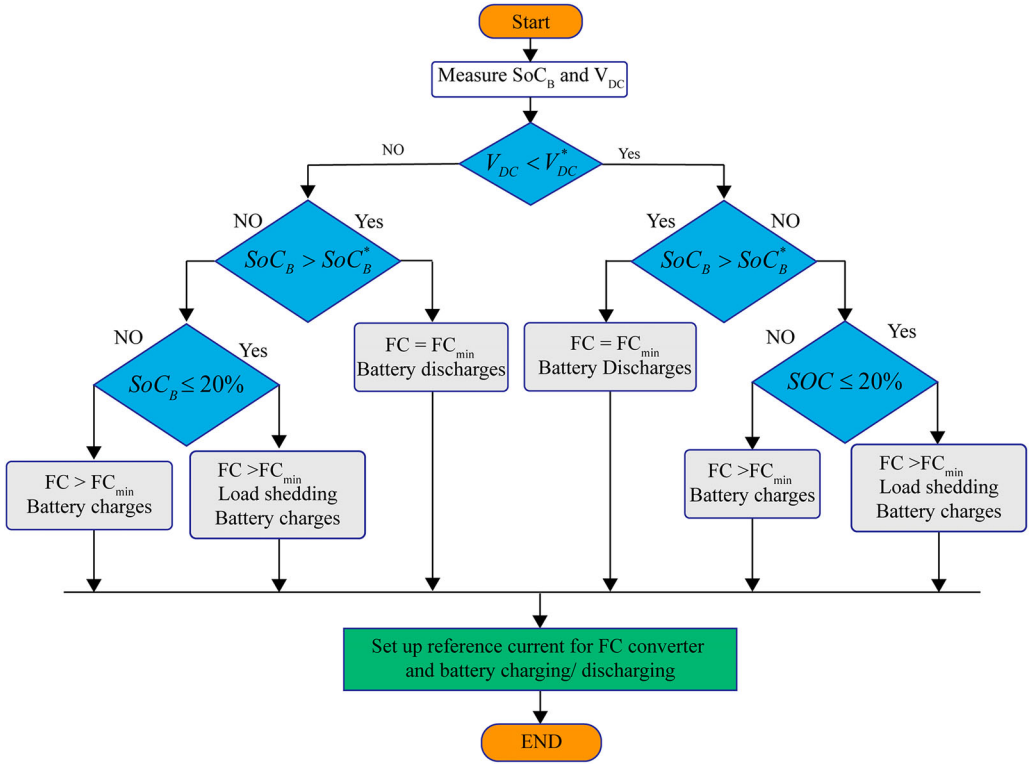

Figure 12. Flowchart of energy management algorithm of DCMG.

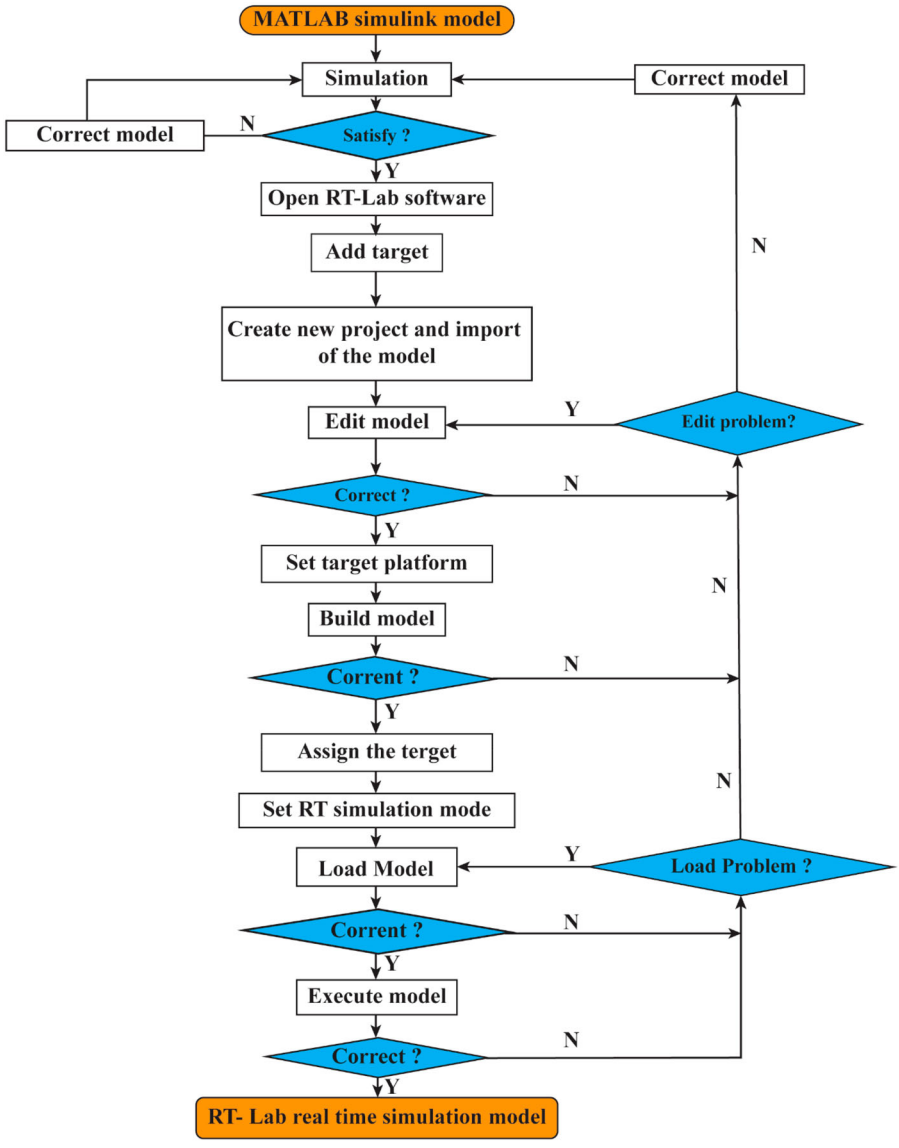

Figure 14. Simulation flow of RT-Lab simulation in real-time.

4. Results and discussion

4.1. Simulations results

The considered microgrid model along with the proposed EMS utilising ANN and PI-based control strategies has been simulated using Simscape™ dynamic module of Matlab®. The simulation involves a run for 250 s with a sample time of 100 µs to compute the model state at the next time step as an explicit function of the current state value and state derivatives using the 4th order Runge–Kutta method. The system performance is analysed in terms of regulation in DBV and active power balance among various components of DCMG including ESDs under desired constraints. To verify the simulation results, system performance was further validated using an experimental setup consisting an FPGA-based real-time simulator opal-RT (OP 5700 RTS), mixed-signal oscilloscope, UPS supply and a host PC. The proposed microgrid setup shown in Figure 16 is tested for the following two conditions:

4.1.1. Case-I, step increments in AC load demand

To examine the effectiveness of the proposed configuration, a simulation study is carried out with step increments in AC load. In contrast, DC load remains constant throughout the operation at 48 Ω, consuming 1.5 kW power. In Figure 17(b), the AC load suddenly changes from 0 to 2 kW at T_1 instant. Consequently, V_{DC} dips proportionately to 268.94 V as in Figure 17(a). From Figure 17(b) it is clear that SC delivers excess power momentarily while FC generates 0.88 kW in steady-state, which is the minimum power produced by FC when SOC_B is greater than 60%, as shown in Figure 18(b). The discrepancy in power is met from SC and battery; as a result, V_{DC} is restored to 270 V. AC load changed swiftly to 3 kW at T_2 moment as shown in Figure 17(b). FC delivers minimum power i.e. 0.88 kW as SOC_B is above its reference value. Battery and SC deliver power through discharging. However, after 117.4 sec, SOC_B reaches below 60%, but the battery still delivers for deficit power by discharging. FC generation as shown in Figure 17(b) takes more time to reach its steady-state

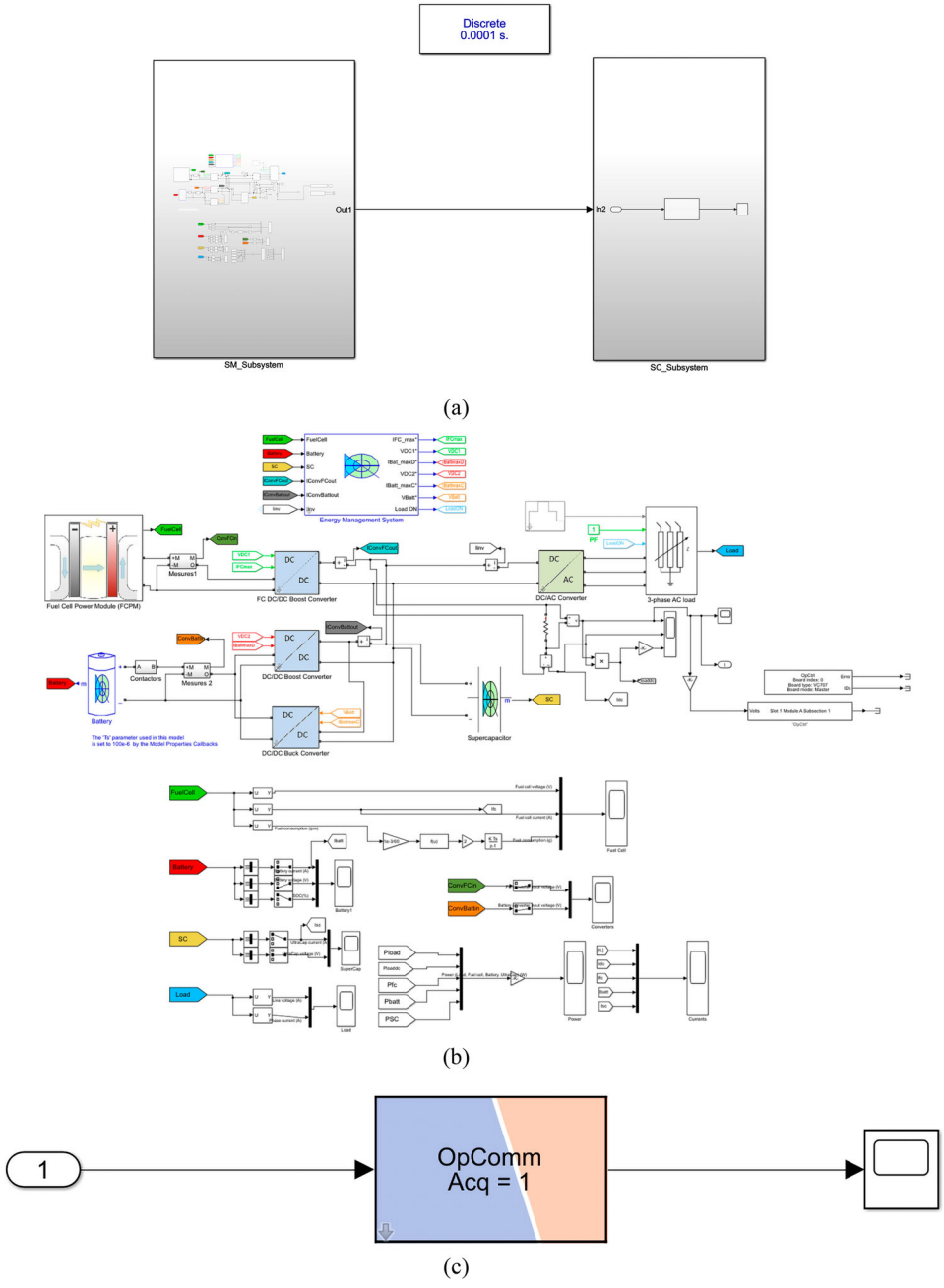

Figure 15. (a) Prepared model for RT-Lab (b) Undermasking view SM_subsystem (c) Undermasking view of SC_subsystem.

as it is a low power density device and power generation from it increases to 4.73 kW at 131.2 s from 0.885 kW at 117.1 s. The battery enters in charging zone at 134 s. V_{DC} drops to 264.27 V as shown in Figure 17(a). SC tries to fix V_{DC} at 270 V by quickly delivering excess power, while the battery takes a longer time to deliver additional power as shown in Figure 17(b). SC delivers instantaneous power whenever there is a sudden change in load, thus reducing battery stresses and enhancing its lifetime. The maximum deviation is 5.72 V, which falls under the 5% band prescribed under *IEEE* standards. Figure 18(a,b) represents battery voltage and SOC_B variation with time.

4.1.2. Case-II, step decrements in AC load demand

In this case, the DC load remains constant throughout the operation at 48 Ω. AC load is decreased in a stepped manner at T_3

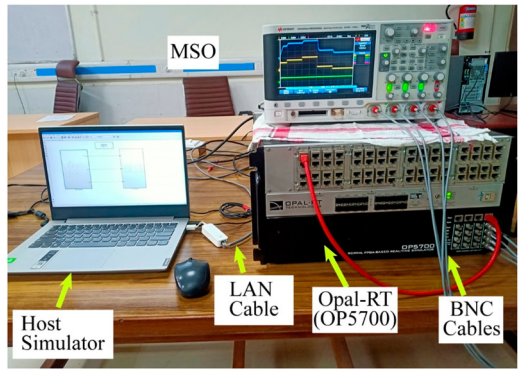

Figure 16. Experimental setup with FPGA- based real-time simulator.

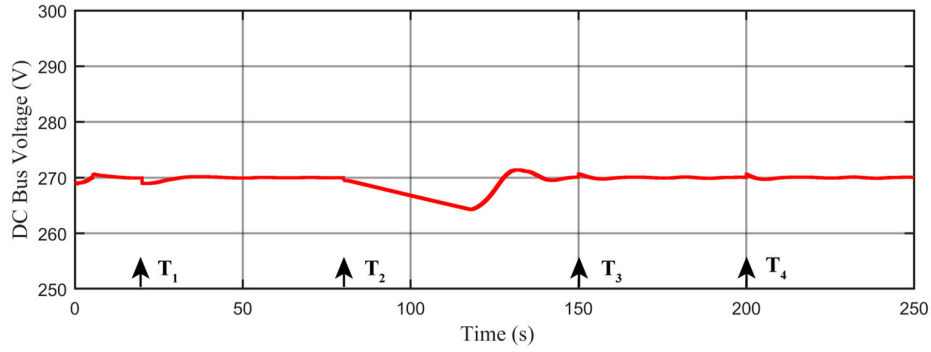

(a)

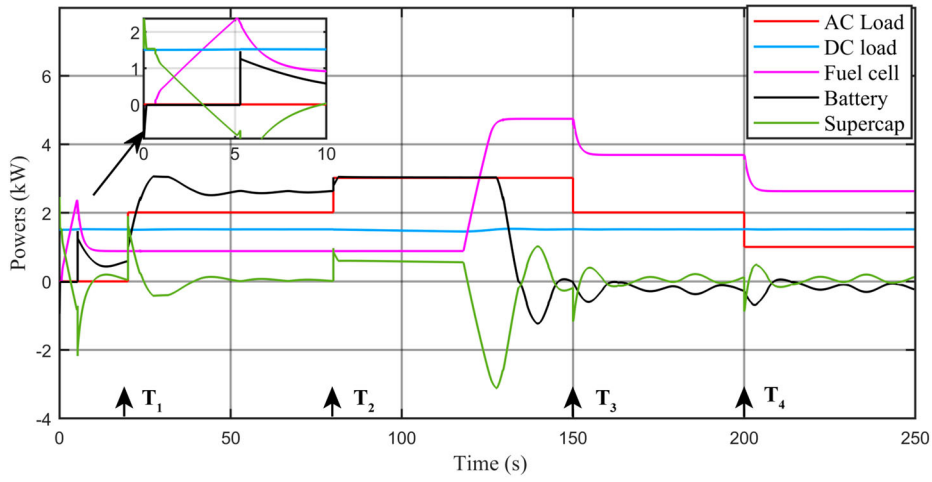

(b)

Figure 17. (a) Simulation results for DBV variations (b) Simulations results for variation in powers.

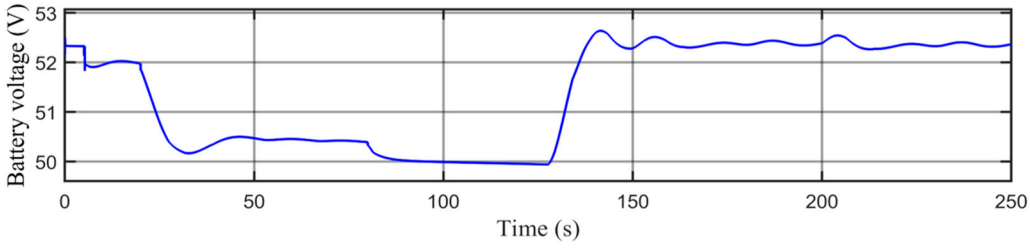

(a)

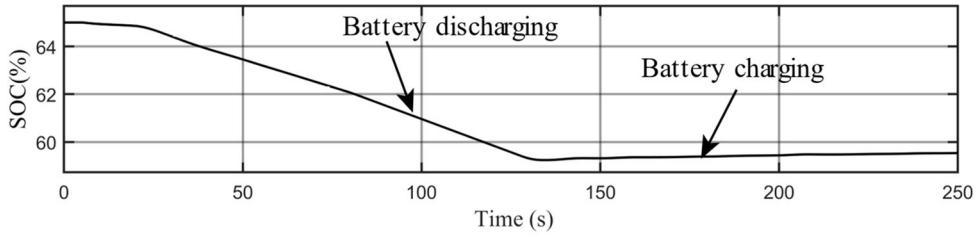

(b)

Figure 18. (a) Battery voltage (b)Battery SOC (%).

and T_4 to 2 and 1 kW, respectively, as shown in Figure 17(b). As a result, DBV increases to 270.20 and 270.66 V at T_3 and T_4, as shown in Figure 17(a). SC momentarily absorbs excess power provided by FC, and thus, DBV is restored to 270 V. In response to a stepped decrease in the AC load at T_3 and T_4, FC delivers 3.69 and 2.63 kW power in steady-state while battery and SC compensate for additional power by charging/discharging in a complementary manner. As shown in Figure 17(b), FC provides power to load, while battery and SC, charge and discharge in a complementary manner. Figure 18(a,b) represents variation in battery voltage and SOC_B against time. The maximum deviation in DBV is ≅ 0.66V, which is within ±5% band as per the *IEEE* std.

4.2. Experimental results

The proposed DCMG incorporating battery and SC as HESS is evaluated using an experimental setup. The experimental desk comprises a host PC, digital signal oscilloscope (DSO), target (OPAL-RT) simulator and UPS supply. Figure 16 shows an experimental setup utilised to validate the robustness of simulation results for the proposed control scheme. Figure 19(a–c) shows

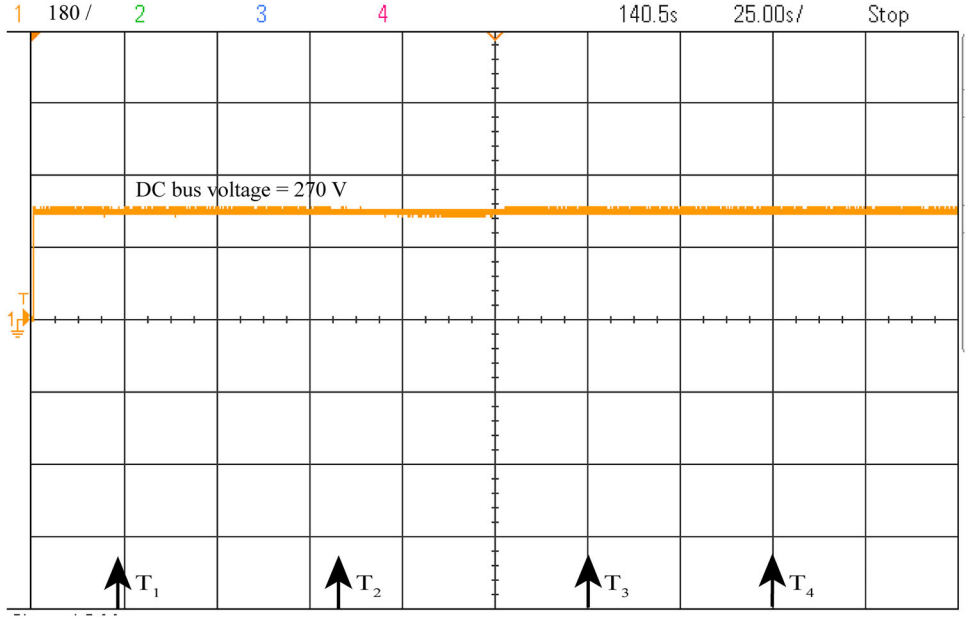

(a)

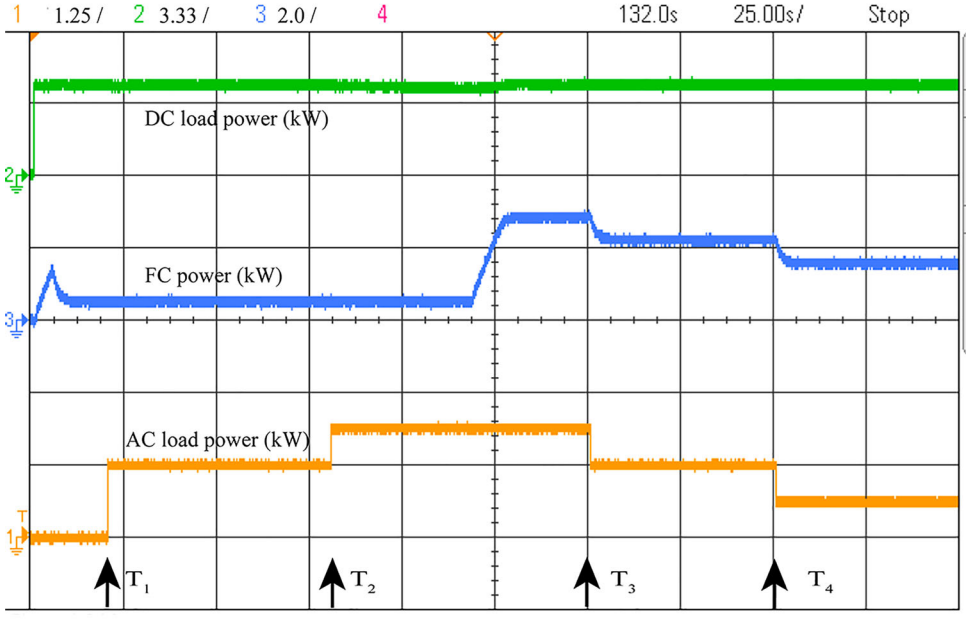

(b)

Figure 19. (a) Experimental results for DBV variation (b) Experimental results for power-sharing among DC, AC load and FC (c) Experimental results for power-sharing between battery and SC.

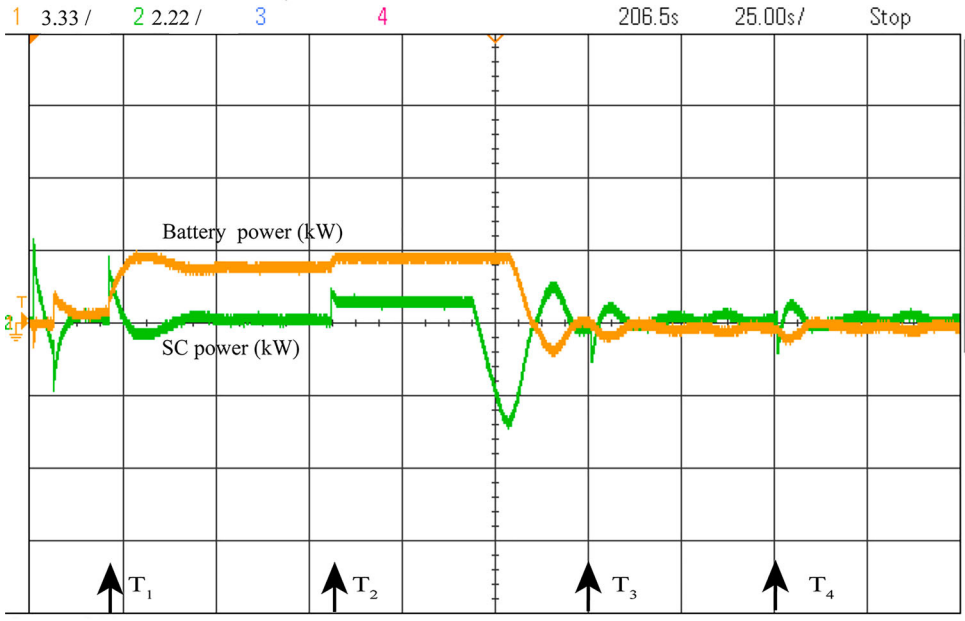

(c)

Figure 19. Continued.

experimental results for V_{DC}, power-sharing among various units of DCMG, respectively. Instant T_1 and T_2 indicate an increase in the AC load indicated for Case-I above. AC load increases at moments T_1 and T_2 while keeping the DC load constant as V_{DC} dips proportionately. However, SC compensates swiftly and maintains the V_{DC} constant. Battery compensates for balance deficits in power by discharging and FC produces minimum power until SOC_B is greater than 60%. FC increases its production when SOC_B drops below 60%. Instant T_3 and T_4 represent the Case-II scenario with a decrease in load. Due to the decrease in load, V_{DC} increases proportionally and SC absorbs surplus power instantaneously generated by FC. In Figure 19 (c), the battery and SC alternately get charged/discharged to compensate surplus power production.

4.3. Performance comparisons between the conventional and proposed controllers

Figure 20(a) shows the generation power of FC with the conventional and proposed ANN controllers demonstrating that the proposed controller outperforms the conventional one in regulating FC power generation. Time response metrics, peak overshoot and settling time in FC power have been analysed for Case-I and Case-II to verify the effectiveness of the proposed control. Figure 20(b,c) depicts a graphic representation of the comparison between the conventional and proposed controllers. It is evident from Figure 20(b,c) that the proposed controller has less overshoot and faster settling time in comparison to the conventional controller.

4.4. Performance comparisons with and without sensor noise

The performance has been compared in terms of deviations in DBV. A noise signal (zero means unit variance white noise) amounting to 1.5 percent of maximum battery SOC as shown in Figure 21, is added to the battery SOC sensor output signal. It is clear from Figure 22(a,b) that the proposed controller outperforms the conventional one in terms of DBV regulation for noisy or degraded information. It is very clear from Figure 22(b) that the proposed ANN controller effectively regulates DBV seamlessly without and with noisy or degraded information. Furthermore, Figure 22(b) shows that the proposed ANN controller works well to control DBV even when the information is noisy or bad, and noise has almost no effect on the actual DBV.

5. Conclusion

EMS and hybrid control strategies comprising ANN and PI controllers for maintaining a constant DBV and effective power sharing among FC, battery and SC were proposed in this paper. An ANN-based controller is designed for controlling FC generation, whereas a PI controller is designed to maintain a constant DBV. EMS for effective power sharing between FC and battery was designed to increase the battery life. The effectiveness of the proposed EMS and hybrid controllers was studied under sudden variations in AC load with and without degraded or noisy information cases. The proposed strategy maintains DBV effectively at its reference value under all situations. The battery and SC are shown to compensate for disparity in power. The ANN controller regulates power generation from FC by varying the duty cycle of the DC/DC boost converter. The proposed EMS was simulated using Simulink® module of Matlab®. The simulation results show a maximum overshoot of 0.5% and a settling time of 80 ms, confirming a significant improvement over the conventional controller. The simulation results also demonstrate the effectiveness of the proposed controller in terms of maximum DBV regulation of 2.11% i.e. within $\pm$ 5% as per IEEE standard

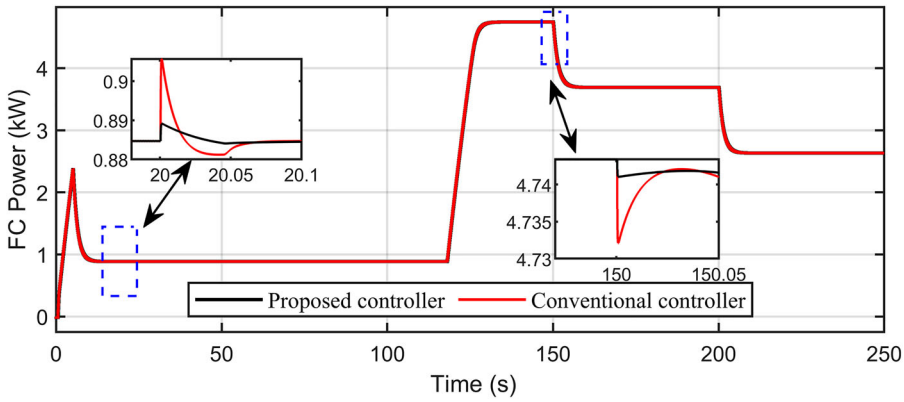

(a)

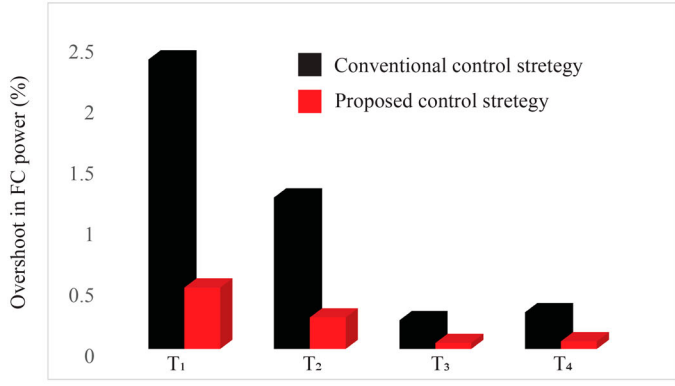

(b)

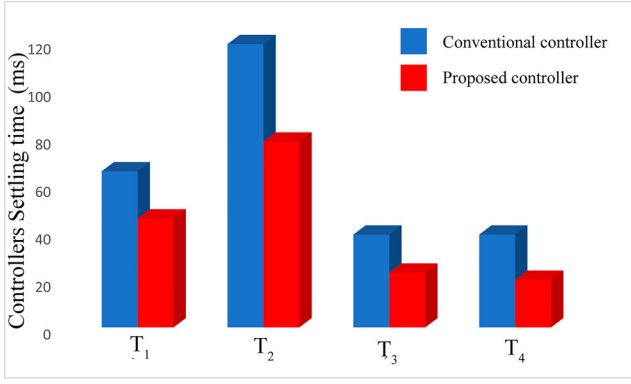

(c)

Figure 20. (a) Simulation results for FC power (b) Performance comparison between conventional and proposed controller for overshoot in FC power (c) Performance comparison based on settling time.

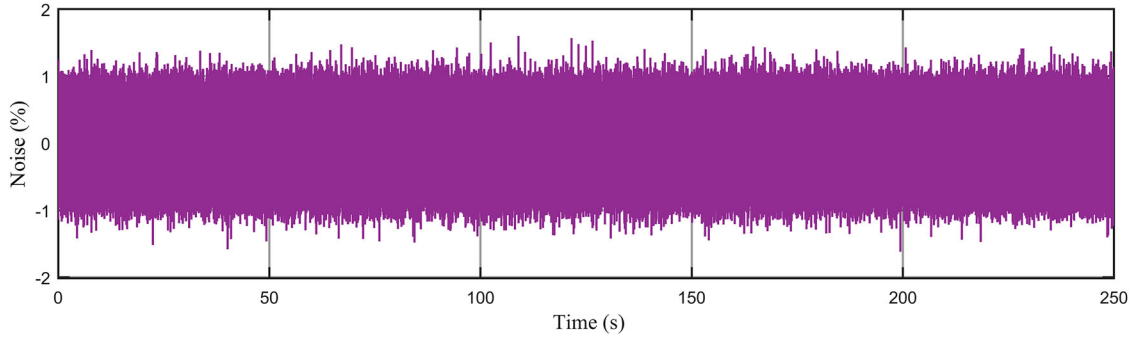

Figure 21. Sensor noise signal.

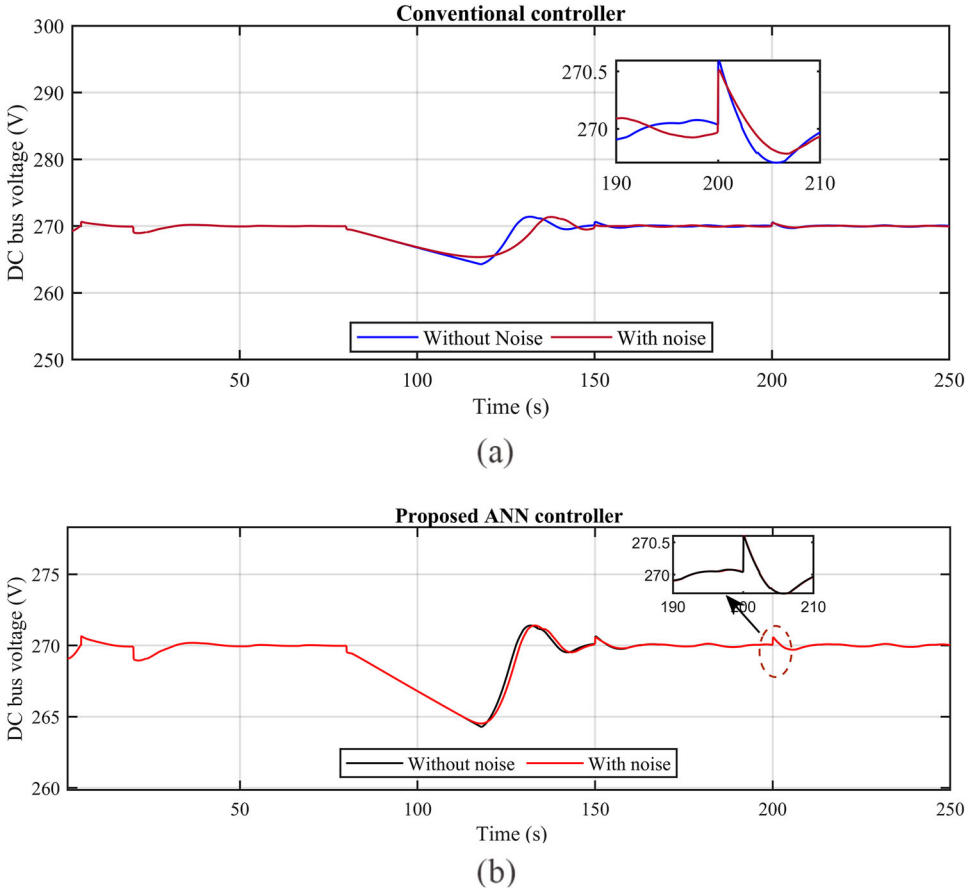

Figure 22. DC bus voltage comparison (a) Conventional controller (b) Proposed controller.

519-1992. The simulation results have been validated using the real-time FPGA-based simulator HIL OPAL-RT (OP5700).

Disclosure statement

No potential conflict of interest was reported by the author(s).

ORCID

Amit Kumar Rajput http://orcid.org/0000-0001-5936-1300

References

Bahloul, M., and S. K. Khadem. 2019, Sept. "Impact of Power Sharing Method on Battery Life Extension in HESS for Grid Ancillary Services." *IEEE Transactions on Energy Conversion* 34 (3): 1317–1327. doi:10.1109/TEC.2018.2886609.

Boujoudar, Y., M. Azeroual, H. El Moussaoui, and T. Lamhamdi. 2020. "Intelligent Controller-Based Energy Management for Stand-Alone Power System Using Artificial Neural Network." *International Transactions on Electrical Energy Systems* 30: e12579. doi:10.1002/2050-7038.12579.

Bracco, Stefano, Federico Delfino, Angela Trucco, and Stefano Zin. 2018. "Electrical Storage Systems Based on Sodium/Nickel Chloride Batteries: A Mathematical Model for the Cell Electrical Parameter Evaluation Validated on a Real Smart Microgrid Application." *Journal of Power Sources* 399: 372–382. doi:10.1016/j.jpowsour.2018.07.115.

Brandt, Robert D., and Feng Lin. 1999. "Adaptive Interaction and its Application to Neural Networks." *Information Sciences* 121 (3–4): 201–215. ISSN 0020-0255. doi:10.1016/S0020-0255(99)00090-0.

Cabrane, Zineb, Jonghoon Kim, Kisoo Yoo, and Mohammed Ouassaid. 2021. "HESS-based Photovoltaic/Batteries/Supercapacitors: Energy Management Strategy and DC bus Voltage Stabilization." *Solar Energy* 216: 551–563. ISSN 0038-092X. doi:10.1016/j.solener.2021.01.048.

Chettibi, N., A. Mellit, G. Sulligoi, and A. Massi Pavan. May 2018. "Adaptive Neural Network-Based Control of a Hybrid AC/DC Microgrid." *in IEEE Transactions on Smart Grid* 9 (3): 1667–1679. doi:10.1109/TSG.2016.2597006.

Christen, Thomas, and Martin W. Carlen. 2000. "Theory of Ragone Plots." *Journal of Power Sources* 91 (2): 210–216. ISSN 0378-77. doi:10.1016/S0378-7753(00)00474-2.

Dicks, Andrew L., and David A. J. Rand. 2018. *Fuel Cell Systems Explained. Fuel Cell Systems Explained*. Wiley. doi:10.1002/9781118706992.

Fu, Zhumu, Zhenhui Li, Pengju Si, and Fazhan Tao. 2019. "A Hierarchical Energy Management Strategy for Fuel Cell/Battery/Supercapacitor Hybrid Electric Vehicles." *International Journal of Hydrogen Energy* 44 (39): 22146–22159. ISSN 0360-3199. doi:10.1016/j.ijhydene.2019.06.158.

Glavin, M. E., P. K. W. Chan, S. Armstrong, and W. G. Hurley. 2008. "A Stand-Alone Photovoltaic Supercapacitor Battery Hybrid Energy Storage System." 13th International Power Electronics and Motion Control Conference, 2008, 1688–1695. doi:10.1109/EPEPEMC.2008.4635510.

Kathiresan, J., S. K. Natarajan, and G. Jothimani. 2020. "Energy Management of Distributed Renewable Energy Sources for Residential DC Microgrid Applications." *International Transactions on Electrical Energy Systems* 30: e12258. doi:10.1002/2050-7038.12258.

Marzougui, Hajer, Ameni Kadri, Jean-Philippe Martin, Mansour Amari, Serge Pierfederici, and Faouzi Bacha. 2019. "Implementation of Energy Management Strategy of Hybrid Power Source for Electrical Vehicle." *Energy Conversion and Management* 195: 830–843. ISSN 0196-8904. doi:10.1016/j.enconman.2019.05.037.

Mishra, Debashish, Prakash Chandra Sahu, Ramesh Chandra Prusty, and Sidhartha Panda. 2021a. "A Fuzzy Adaptive Fractional Order-PID Controller for Frequency Control of an Islanded Microgrid Under Stochastic Wind/Solar Uncertainties." *International Journal of Ambient Energy*. doi:10.1080/01430750.2021.1914163.

Mishra, Debashish, Prakash Chandra Sahu, Ramesh Chandra Prusty, and Sidhartha Panda. 2021b. "Power Generation Monitoring of a Hybrid

Power System with I-GWO Designed Trapezoidal Type-II Fuzzy Controller." *International Journal of Modelling and Simulation* 42: 5, 797–5, 813. doi:10.1080/02286203.2021.1983744.

Nouman, K., Z. Asim, and K. Qasim. 2018. "Comprehensive Study on Performance of PID Controller and its Applications," 2018 2nd IEEE Advanced Information Management,Communicates,Electronic and Automation Control Conference (IMCEC), 1574–1579. doi:10.1109/IMCEC.2018.8469267.

Papari, B., C. S. Edrington, I. Bhattacharya, and G. Radman. 2019. "Effective Energy Management of Hybrid AC–DC Microgrids With Storage Devices." *in IEEE Transactions on Smart Grid* 10 (1): 193–203, January. doi:10.1109/TSG.2017.2736789.

Pradhan, C., M. K. Senapati, S. G. Malla, P. K. Nayak, and T. Gjengedal. 2021. "Coordinated Power Management and Control of Standalone PV-Hybrid System With Modified IWO-Based MPPT." *in IEEE Systems Journal* 15 (3): 3585–3596, September. doi:10.1109/JSYST.2020.3020275.

Rahman, Md Mustafizur, Abayomi Olufemi Oni, Eskinder Gemechu, and Amit Kumar. 2020. "Assessment of Energy Storage Technologies: A Review." *Energy Conversion and Management* 223: 113295. ISSN 0196-8904. doi:10.1016/j.enconman.2020.113295.

Sahoo, S. K., A. K. Sinha, and N. K. Kishore. June 2018. "Control Techniques in AC, DC, and Hybrid AC–DC Microgrid: A Review." *in IEEE Journal of Emerging and Selected Topics in Power Electronics* 6 (2): 738–759. doi:10.1109/JESTPE.2017.2786588.

Sahu, Prakash Chandra, Reetimukta Baliarsingh, Ramesh Chandra Prusty, and Sidhartha Panda. 2020c. "Novel DQN Optimised Tilt Fuzzy Cascade Controller for Frequency Stability of a Tidal Energy-Based AC Microgrid." *International Journal of Ambient Energy* 43 (1): 3587–3599. doi:10.1080/01430750.2020.1839553.

Sahu, Prakash Chandra, Sonalika Mishra, Ramesh Chandra Prusty, and Sidhartha Panda. 2018. "Improved-salp Swarm Optimized Type-II Fuzzy Controller in Load Frequency Control of Multi Area Islanded AC Microgrid." *Sustainable Energy, Grids and Networks* 16: 380–392. ISSN 2352-4677. doi:10.1016/j.segan.2018.10.003.

Sahu, Prakash Chandra, Ramesh Chandra Prusty, and Sidhartha Panda. 2020a. "Frequency Regulation of an Electric Vehicle-Operated Micro-Grid Under WOA-Tuned Fuzzy Cascade Controller." *International Journal of Ambient Energy* 43: 1, 2900–1, 2911. doi:10.1080/01430750.2020.1783358.

Sahu, Prakash Chandra, Ramesh Chandra Prusty, and Sidhartha Panda. 2020b. "Optimal Design of a Robust FO-Multistage Controller for the Frequency Awareness of an Islanded AC Microgrid Under i-SCA Algorithm." *International Journal of Ambient Energy* 43 (1): 2681–2693. doi:10.1080/01430750.2020.1758783.

Sankar, Yannam Ravi, and K. Chandra Sekhar. 2021. "Design and Control of Hybrid Energy Microgrid System Using Renewable Energy Sources." *International Journal of Ambient Energy*, doi:10.1080/01430750.2021.1909653.

Shaikh, U. A., M. K. AlGhamdi, and H. A. AlZaher. 2018. "Novel Product ANFIS-PID Hybrid Controller for Buck Converters." *The Journal of Engineering*, 730–734. doi:10.1049/joe.2018.0113.

Singh, P., and J. S. Lather. 2018. "A PWM-Based Sliding Mode Voltage Control of DC-DC Boost Converter for DC Microgrid." IEEE 8th Power India International Conference (PIICON), 2018, 1–5. doi:10.1109/POWERI.2018.8704456.

Singh, Prashant, and J. S. Lather. 2019. "Artificial Neural Network-Based Dynamic Power Management of a DC Microgrid: A Hardware-in-Loop Real-Time Verification." *International Journal of Ambient Energy* 43 (1): 1730–1738. doi:10.1080/01430750.2020.1720811.

Singh, Prashant, and J. S. Lather. 2020. "Dynamic Current Sharing, Voltage and SOC Regulation for HESS Based DC Microgrid Using CPISMC Technique." *Journal of Energy Storage* 30: 101509. ISSN 2352-152X. doi:10.1016/j.est.2020.101509.

Sinha, Smita, and Prabodh Bajpai. 2020. "Power Management of Hybrid Energy Storage System in a Standalone DC Microgrid." *Journal of Energy Storage* 30: 101523. ISSN 2352-152X. doi:10.1016/j.est.2020.101523.

Soumeur, Mohammed Amine, Brahim Gasbaoui, Othmane Abdelkhalek, Jamel Ghouili, Tofik Toumi, and Abdeselem Chakar. 2020. "Comparative Study of Energy Management Strategies for Hybrid Proton Exchange Membrane Fuel Cell Four Wheel Drive Electric Vehicle." *Journal of Power Sources* 462: 228167. ISSN 0378-7753. doi:10.1016/j.jpowsour.2020.228167.

Vu, Tuyen V., Dallas Perkins, Fernand Diaz, David Gonsoulin, Chris S. Edrington, and Touria El-Mezyani. 2017. "Robust Adaptive Droop Control for DC Microgrids." *Electric Power Systems Research* 146: 95–106. ISSN 0378-7796. doi:10.1016/j.epsr.2017.01.021.

Xu, D., Q. Liu, W. Yan, and W. Yang. 2019. "Adaptive Terminal Sliding Mode Control for Hybrid Energy Storage Systems of Fuel Cell, Battery and Supercapacitor." *in IEEE Access* 7: 29295–29303. doi:10.1109/ACCESS.2019.2897015.